
Phase 2 Study of ^{99m}Tc -Trofolastat SPECT/CT to Identify and Localize Prostate Cancer in Intermediate- and High-Risk Patients Undergoing Radical Prostatectomy and Extended Pelvic LN Dissection

Karolien E. Goffin¹, Steven Joniau², Peter Tenke³, Kevin Slawin⁴, Eric A. Klein⁵, Nancy Stambler⁶, Thomas Strack⁶, John Babich⁷, Thomas Armor⁶, and Vivien Wong⁶

¹Nuclear Medicine, UZ Leuven, Department of Imaging and Pathology, KU Leuven, Leuven, Belgium; ²Urology, UZ Leuven, Department of Development and Regeneration, KU Leuven, Leuven, Belgium; ³Jahn Ferenc South Pest Hospital, Budapest, Hungary; ⁴University of Texas Vanguard Urologic Institute, Houston, Texas; ⁵Glickman Urological and Kidney Institute, Cleveland Clinic Foundation, Cleveland, Ohio; ⁶Progenics Pharmaceuticals, New York, New York; and ⁷Weill Cornell Medicine, New York, New York

^{99m}Tc -trofolastat (^{99m}Tc -MIP-1404), a small-molecule inhibitor of prostate-specific membrane antigen, shows high potential to detect prostate cancer (PCa) noninvasively using SPECT. We therefore wanted to assess the performance of ^{99m}Tc -trofolastat SPECT/CT in a phase 2 multicenter, multireader prospective study in patients with intermediate- and high-grade PCa, before radical prostatectomy and extended pelvic lymph node (LN) dissection, with histopathology as the gold standard. **Methods:** PCa patients ($n = 105$) with an increased risk of LN involvement (LNI) underwent pelvic ^{99m}Tc -trofolastat SPECT/CT before radical prostatectomy with extended pelvic LN dissection. The sensitivity of ^{99m}Tc -trofolastat for detection of PCa on a patient and lobe basis, using visual and semi-quantitative (tumor-to-background ratio [TBR]) scores, and of LNI was evaluated as well as the correlation of uptake within the gland to Gleason scores (GS) and assessment of the predictive potential of ^{99m}Tc -trofolastat uptake for LNI. **Results:** PCa was detected in 98 patients (94%) with acceptable variability between readers. There was a significantly higher visual score and TBR in positive lobes compared with tumor-negative lobes. Receiver-operating characteristic analysis showed that visual scores more accurately discriminated lobes with $\text{GS} \leq 3 + 3$ from $\geq 3 + 4$, whereas TBRs discriminated high-grade disease from normal lobes better. Visual scores and TBRs correlated significantly with GS. ^{99m}Tc -trofolastat SPECT/CT detected LNI with a sensitivity of 50% and specificity of 87%, and TBR values significantly predicted LNI with a sensitivity of 90%. **Conclusion:** ^{99m}Tc -trofolastat SPECT/CT detects PCa with high sensitivity in patients with intermediate- and high-risk PCa compared with histology. It has the potential to be used as a surrogate marker for GS and predict LNI.

Key Words: ^{99m}Tc -trofolastat (^{99m}Tc -MIP-1404); SPECT/CT; prostate cancer; histopathology

J Nucl Med 2017; 58:1408–1413
DOI: 10.2967/jnumed.116.187807

Imaging plays an increasingly important role in the initial diagnosis of prostate cancer (PCa). Multiparametric MRI of the prostate is an emerging tool for accurate localization of the tumor within the prostate gland as well as for evaluating the extension of disease into neighboring tissues (1), but nuclear medicine techniques have also shown potential in the diagnosis and primary staging of PCa (2). One of the most recent developments within this field has been the development of radiotracers targeting prostate-specific membrane antigen (PSMA), a transmembrane 750 amino acid type II glycoprotein and zinc metalloenzyme that is primarily expressed in normal human prostate epithelium. PSMA is upregulated in PCa relocated from the cytosol to the cell membrane, thus becoming accessible to targeted binding by substrates or antibodies (3,4). Because PSMA is expressed by virtually all PCa and its expression is further increased in poorly differentiated, metastatic, and hormone-refractory PCa, it is an attractive target for diagnosis and staging of this disease (5–11). Apart from radiotracers for imaging with PET, such as ^{68}Ga -labeled Glu-urea-Lys(Ahx)-HBED-CC (^{68}Ga -HBED-CC or ^{68}Ga -PSMA-11) or 2-(3-(1-carboxy-5-[(6-[^{18}F]fluoro-pyridine-3-carbonyl)-amino]-pentyl)-ureido)-pentanedioic acid (^{18}F -DCFPyL) (12–15), small-molecule inhibitors of PSMA labeled with ^{99m}Tc have been developed for imaging with SPECT (16–18), a nuclear medicine imaging technique that is more widely available than PET. Two variants of ^{99m}Tc -trofolastat, ^{99m}Tc -MIP-1404 and ^{99m}Tc -MIP-1405, were shown to have favorable biodistribution and kinetic behavior and visualized metastatic lesions in bone, prostate bed, and lymph nodes (LNs) in patients with metastatic PCa (19). Because prior work established that ^{99m}Tc -MIP-1404 had minimal activity in the bladder and had higher uptake in suspected lesions, this agent was chosen for use in the current study. To assess the performance characteristics of ^{99m}Tc -MIP-1404 (in the following ^{99m}Tc -trofolastat) imaging, we performed a phase 2 multicenter, multireader prospective study comparing imaging with histopathology as the gold standard, in patients with intermediate- and high-grade primary PCa, subsequent to radical prostatectomy and extended pelvic LN dissection. The primary study objective was detection of disease at the gland level compared with histopathology. Secondary study objectives were evaluation of the location and the extent of disease within the prostate gland and the prediction of LN status based on imaging.

Received Jan. 3, 2017; revision accepted Mar. 1, 2017.
For correspondence or reprints contact: Karolien Goffin, Nuclear Medicine, University Hospital Leuven, Herestraat 49, 3000 Leuven, Belgium.
E-mail: Karolien.goffin@uzleuven.be
Published online Mar. 16, 2017.
COPYRIGHT © 2017 by the Society of Nuclear Medicine and Molecular Imaging.

MATERIALS AND METHODS

Patients

From September 2012 to October 2013, 105 patients with histologically proven adenocarcinoma of the prostate gland and at high risk for LN metastases by a stage of cT3, cT4, or a total nomogram score of 130 or more (20), who were scheduled to undergo radical prostatectomy with extended pelvic LN dissection, were prospectively included in this multicenter study. A complete medical history including tumor grade, clinical stage, and prostate-specific antigen; any past or present PCa therapies; and demographic information was collected. The local ethics committees approved the study, and written informed consent was obtained from all patients before inclusion (NCT01667536). Baseline characteristics of the study population can be found in Table 1.

Pelvic MRI

At least 1 d before study drug administration, patients underwent contrast-enhanced MRI of the pelvis (T1- and T2-weighted images with at least a 1.5 T magnet using a torso phased-array coil or combined endorectal-body phased-array coil). Sequences included axial and

coronal pre- and postcontrast fat saturation protocols with a slice thickness of 5 mm or less.

^{99m}Tc-Trofolostat Imaging

In this study, an optimized and simplified method was used to radiolabel the drug precursor with ^{99m}Tc, compared with the labeling procedure that has been described earlier (19). Three to 6 h before imaging, an activity of 740 ± 111 MBq of ^{99m}Tc-trofolostat was injected intravenously. Simultaneous anterior and posterior whole-body scans were obtained using a scan speed of 10 cm/min. This was followed by a pelvic dual-head SPECT/CT (step-and-shoot, 30 s per stop, 60–64 projections per head; CT 130 kVp, 10–30 mAs). SPECT acquisitions were iteratively reconstructed on a commercially available workstation (Segami) using ordered-subset expectation maximization, applying scatter correction and CT-based attenuation correction at ICON Medical Imaging.

Surgery

Patients underwent a standard of care radical prostatectomy with a standardized extended pelvic LN dissection including obturator and iliac regions, at least 1 wk, but no more than 3 wk, after ^{99m}Tc-trofolostat imaging. Surgical staff was masked to the results of ^{99m}Tc-trofolostat imaging and labeled all specimens to correlate to the specific anatomic location of removal.

Surgical Pathology

Immediately after surgery, specimens were prepared for local histopathologic processing and analysis using a study-specific pathology manual. Briefly, gross handling of the prostate gland and lymphadenectomy specimens included whole mount assessment and sectioning of the prostate gland, overall measurement of specimen size, palpation to identify LNs in fatty tissue, dissection and description of identified LNs, and submission of LNs in their entirety plus all remaining fibroadipose tissue for each harvested regional packet.

Image Analysis

^{99m}Tc-trofolostat images were evaluated centrally and independently by 3 board-certified nuclear medicine physicians, masked to clinical information. Each reviewer received a brief training session, which included review of 10–20 normal and abnormal cases from previous clinical trials.

For visual evaluation of ^{99m}Tc-trofolostat uptake within the prostate gland, a binary evaluation of the presence or absence of increased uptake was made. For semiquantitative evaluation of ^{99m}Tc-trofolostat uptake, the tumor-to-background ratio (TBR) was calculated for each visually detected lesion or other tissue within each lobe (right/left) of the prostate using the quotient of maximal counts within a circular region of interest and mean counts within the obturator muscle (Supplemental Fig. 1 [supplemental materials are available at <http://jnm.snmjournals.org>]). Furthermore, a detailed visual scoring scale was used to score uptake in each lobe (right/left) with higher scores representing more intense levels of uptake, as judged by the TBR (Supplemental Table 1). For LN assessment, abnormal LN uptake was defined as abnormal distribution of activity in tissues and organs greater than local background and consistent with sites of PCa metastatic spread, and consensus between readers was defined as the agreement of at least 2 of the readers for each case.

Contrast-enhanced T1- and T2-weighted MR images of the pelvis and available functional sequences were evaluated centrally by an experienced radiologist masked to clinical information. Each patient with evaluable images was assessed for the presence or absence of PCa at the level of the whole prostate gland, right and left lobes of the prostate gland, and pelvic LNs.

TABLE 1

Baseline Characteristics of Study Population

Characteristic	Value
Mean age (y)	63.2 (range, 46–77)
Clinical T-stage (n)	
T1c	1 (1)
T2	2 (1.9)
T2a	7 (6.7)
T2b	32 (30.5)
T2c	20 (19)
T3	4 (3.8)
T3a	29 (27.6)
T3b	10 (9.5)
Race (n)	
White	102 (97.1)
Black	2 (1.9)
Asian	1 (1)
Mean prostate-specific antigen (ng/mL)	27.0 (range, 2.4–372.7)
Prostate-specific antigen (n)	
≤20	68 (65)
2	36 (35)
Mean GS	8 (range, 6–9)
Biopsy GS (n)	
≤6	5 (5)
7	41 (39)
≥8	59 (56)
Enrollment patients (n)	
United States	40 (38)
Europe	65 (63)
Ongoing ADT (n)	20

Data in parentheses are percentages unless otherwise indicated.

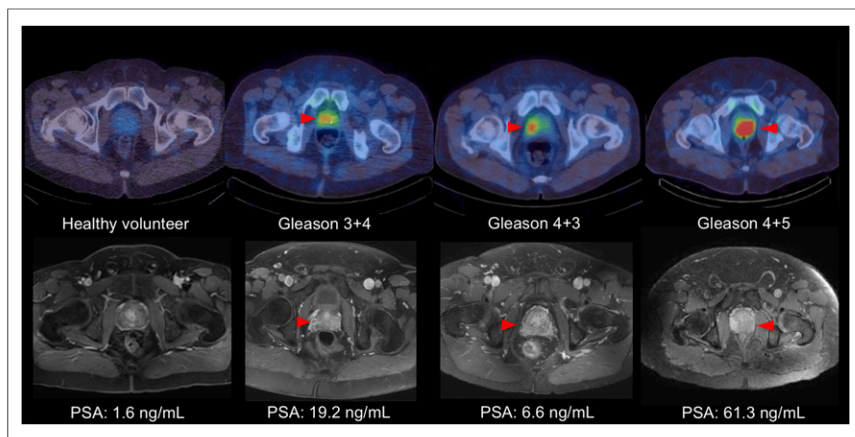


FIGURE 1. Examples of fused axial ^{99m}Tc -trofolostat SPECT/CT reconstructions from previously acquired healthy volunteer (first column) and 3 study patients (top row), and matching axial contrast-enhanced T1-weighted MR images (bottom row) arranged by GS from left to right. Red arrowheads indicate location of histologically confirmed primary prostate lesions.

Statistical Analysis

The primary analysis estimated the ability of ^{99m}Tc -trofolostat to detect histologically confirmed PCa in the prostate and was based on the calculation of the percentage of positive ^{99m}Tc -trofolostat scans of the whole prostate, using histopathology results as the gold standard. The true-positive fraction (equivalent to sensitivity) was calculated. Secondary efficacy parameters involved the calculation of the false-positive fraction (equivalent to $1 - \text{specificity}$) of ^{99m}Tc -trofolostat compared with histopathology within the prostate gland (lobe level). The Spearman correlation coefficient was used to assess associations between TBR and visual scores and postprostatectomy GS. Student *t* tests were performed between mean values of TBR of positive and negative findings, GS, and prior treatment across each independent reader and the average of 3 readers. Median visual scores were tested using a Wilcoxon rank-sum test. For all analyses, a *P* value of less than 0.05 was considered significant. Receiver-operating characteristic (ROC) analyses and areas under the curve (AUCs) with corresponding 95% confidence intervals were calculated for TBR and reader scores using positive and negative controls of any PCa, $\text{GS} > 3 + 4$, and LNI and optimal cutoff values determined by Youden's *J* statistic. Statistical analysis was performed using R version 3.2.1 (R Foundation for Statistical Computing). Spearman correlation and the Wilcoxon rank-sum test were calculated using JMP (version 11.2.0; SAS Institute Inc.).

RESULTS

Detection of PCa Within Prostate Gland

From the 105 patients of the study population, SPECT/CT images of 104 patients were available for evaluation. One patient did not undergo SPECT/CT imaging, 1 other patient underwent only SPECT imaging and was excluded for semiquantitative analysis, and 6 patients did not have an evaluable MRI.

On a patient basis, PCa was detected by a consensus of at least 2 of the 3 readers in 98 of 104 patients (94%) using ^{99m}Tc -trofolostat SPECT/CT and confirmed by histopathologic findings. There was an acceptable variability in true-positive fraction between readers: 89%, 85%, and 98%, respectively. MRI and ^{99m}Tc -trofolostat SPECT/CT results could be compared in 98 patients. In this subgroup, detection rates were 94% and 86% for SPECT/CT and MRI, respectively. Because all patients were confirmed by pathologic evaluation to have adenocarcinoma of the prostate gland, false-

positive fraction could not be calculated on a patient basis. Representative examples of positive ^{99m}Tc -trofolostat SPECT/CT images can be seen in Figure 1.

Of 206 evaluable prostate lobes, 24 were normal by histopathology (13 right, 11 left) and were used as controls in further analyses. Compared with control lobes, there was a significantly higher median visual score in positive lobes (3.0 vs. 0, $P < 0.0001$) (Fig. 2; Supplemental Table 2). Semiquantitative analysis showed significantly higher average TBRs in PCa-positive lobes than control lobes (26.1 vs. 13.5, $P < 0.0015$) (Fig. 2).

ROC analysis of the median visual scores showed a similar AUC of 0.74 for discrimination of any PCa per lobe and 0.72 for areas of the gland containing $\text{GS} \geq 3 + 4$ disease (Fig. 3) with optimal cutoff values of 2.5 and 3.5, respectively. Conversely,

ROC analysis of semiquantitative TBRs showed AUCs between 0.70 and 0.78, with a lower AUC value for detection of any grade PCa than areas of the gland containing $\text{GS} \geq 3 + 4$ disease (Fig. 3) and optimal cutoff values of 12 and 20, respectively.

Correlation of ^{99m}Tc -Trofolostat Uptake to GS

Median visual scores were significantly higher in PCa-positive lobes with $\text{GS} \geq 3 + 4$ than $\leq 3 + 3$ (4.0 vs. 1.0, $P < 0.0001$), as were TBRs (30.8 vs. 13.1, $P < 0.0001$) (Figs. 1 and 2). Moreover, the average visual score correlated significantly with GS (Spearman $\rho = 0.48$, $P < 0.0001$), as did TBRs (Spearman $\rho = 0.53$, $P < 0.0001$) (Fig. 4).

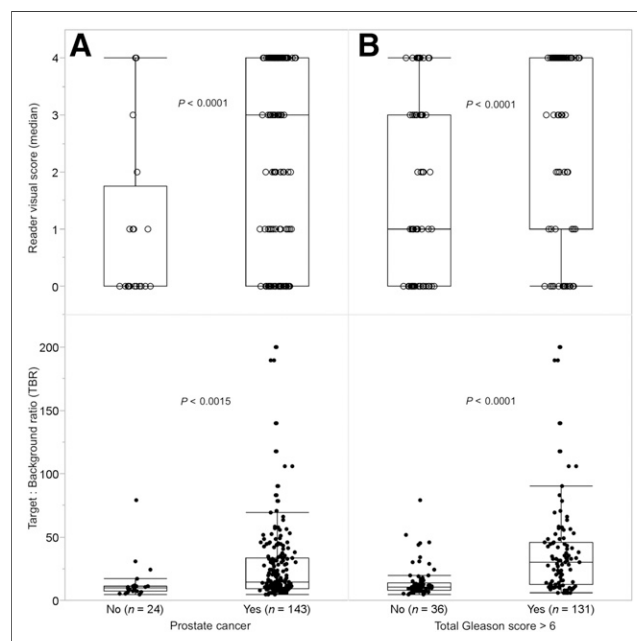


FIGURE 2. Box-and-whisker plots of mean reader scores (top row, \circ) and TBR values (bottom row, \bullet) in prostate lobes: without PCa and with PCa (A); with $\text{GS} \leq 6$ and $\text{GS} \geq 7$ (B). Box and whiskers represent mean and interquartile range.

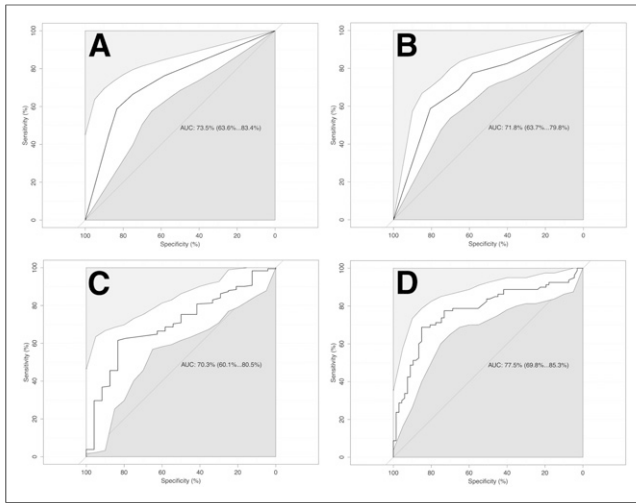


FIGURE 3. ROC analyses curves and 95% confidence intervals (white area) of semiquantitative scoring system (A) and TBR (B) for detection of any grade PCa and semiquantitative scoring system (C) and TBR (D) for detection of GS ≥ 7 (3 + 4).

LN Assessment

A total of 3,025 nodes were removed from 103 patients (mean, 29.6; range, 1–88). Of these, 79 nodes were positive by pathology in 33 patients (32%). A representative example of accurately detected LNI can be seen in Supplemental Figure 2. At the patient level, sensitivity and specificity for detection of LN invasion were 33.3% and 88.4%, respectively. When patients who were currently being treated with androgen-deprivation therapy (ADT) were excluded, sensitivity and specificity increased to 50.0% and 87.3%, respectively. On MRI, sensitivity and specificity for detection of LN invasion were 12.5% and 95.5% in all patients, and 15.8% and 96.2% when patients who were receiving ADT were excluded.

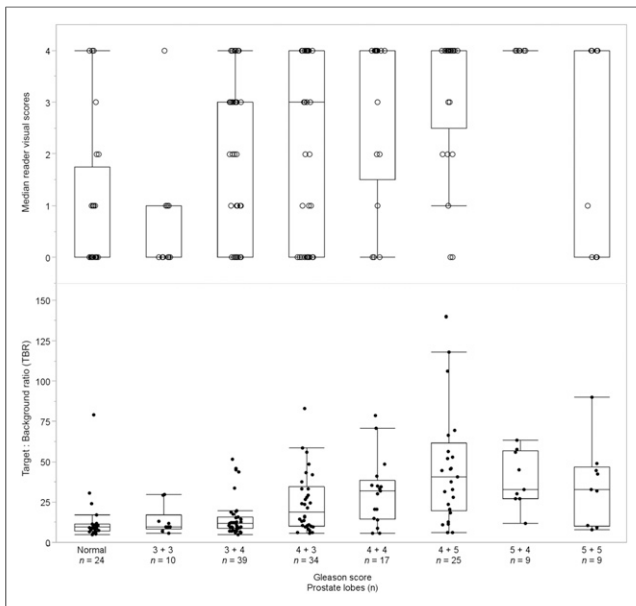


FIGURE 4. Box-and-whisker plots of mean reader scores (top row, \circ) and TBR values (bottom row, \bullet) in lobes with no PCa and in lobes with PCa of increasing GS.

TBR values of the prostatic lesion were found to be a predictor of LNI in evaluable treatment-naïve patients. ROC analysis showed an overall diagnostic accuracy of 77% (AUC, 0.77; 95% confidence interval, 0.65–0.89) with a cutoff of 30.2 (Fig. 5). This yielded a sensitivity of 90% (18/20) and specificity of 67% (37/55) for the presence of LNI after a standardized extended pelvic LN dissection.

DISCUSSION

In this multicenter prospective phase 2 study, we demonstrate that ^{99m}Tc -trofolastat (^{99m}Tc -MIP1404) SPECT/CT imaging is able to detect varying degrees of primary PCa with high accuracy, confirmed by postoperative histopathology of the primary tumor and LNs. Increased uptake within the tumoral lesion was detected in 94% of patients, compared with 86% considered abnormal on MRI. However, mainly standard anatomic T1- and T2-weighted MR sequences were used in this study to evaluate the whole pelvis, which may explain the lower detection rate of MRI in primary lesions. Eiber et al. found that ^{68}Ga -PSMA PET (detection rate, 92%) outperformed multiparametric MRI (detection rate, 66%) to detect primary PCa in 53 eligible patients. Combined ^{68}Ga -PSMA PET/MRI showed an even higher detection rate (98%) (21). Giesel et al. found good allocation of PCa in accordance to biopsy with multiparametric MRI as well as ^{68}Ga -PSMA PET/CT in 10 patients with primary PCa with visually concordant tumor extension on ^{68}Ga -PSMA PET/CT using an isocontour 50% of SUV_{max} compared with multiparametric MRI (22). Contrasting results were described by Rowe et al., who found a higher sensitivity for MRI than for ^{18}F -DCFBC PET in detecting primary PCa of variable GS (6–9) in a segment-based analysis in 13 patients. Specificity, on the other hand, was higher for ^{18}F -DCFBC PET, especially for high-grade lesions with a volume larger than 1.0 mL (23).

Image interpretation of ^{99m}Tc -trofolastat SPECT/CT images was performed by 3 readers with no prior experience with ^{99m}Tc -trofolastat and was proven to be easy and reliable, because detection rates and visual scores had acceptable variability. Visual reader scores as well as semiquantitative TBRs were significantly higher in PCa-positive lobes than normal lobes. ROC analysis demonstrated that quantitative scoring in the form of TBR may be better for discriminating higher-grade PCa from normal prostate tissue, whereas semiquantitative visual scoring appeared to better differentiate normal tissue and low-grade PCa with a GS $\leq 3 + 3$ from higher-grade PCa with a GS $\geq 3 + 4$. This finding suggests that readers used other visual information such as the pattern of uptake as an additional cue in borderline cases with lower TBR values.

In line with previous findings in which higher PSMA expression was seen with increasing tumor aggressiveness (24), ^{99m}Tc -trofolastat uptake in prostate lesions was correlated to GS with higher visual reader scores and higher TBRs at higher GS. When PSMA PET imaging was used, contrasting results have been described, with a significant correlation between GS and tracer uptake in several studies (23,25,26) and no significant correlation in others (21,27). Similarly, it has been shown that both apparent diffusion coefficient and MR spectroscopy are correlated with Gleason grade (28–30). Thus, there is a potential role for ^{99m}Tc -trofolastat imaging not only in localizing tumor but also in identifying areas of more aggressive tumor that could be targeted by transrectal ultrasound- or MRI-guided prostate biopsy or used to guide repeated prostate biopsy in patients with previous negative biopsies, thus improving medical decisions.

At present, LN dissection is still the only reliable staging tool for LNI in high-risk PCa, because nomograms lack accuracy. On a

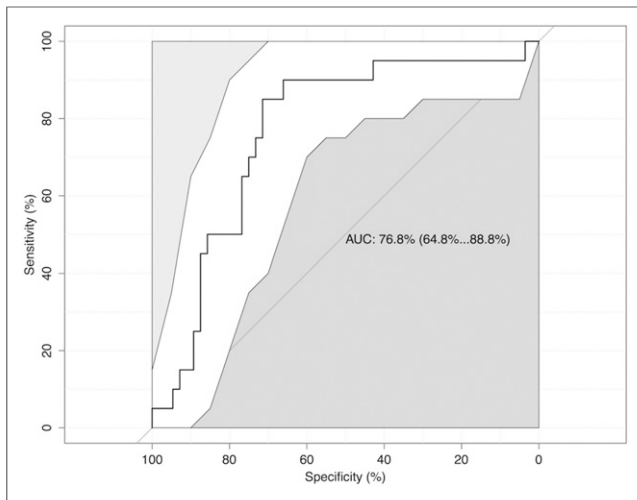


FIGURE 5. ROC analysis curves and 95% confidence intervals (white area) of TBR of prostate lesion using a TBR cutoff of 30.2 to predict presence of LNI. Maximal AUC is 0.77, yielding a sensitivity of 90% and a specificity of 67%.

patient level, ^{99m}Tc -trofolostat imaging shows a low sensitivity, but good specificity at detecting LNI. These findings are in line with previous studies. Budaüs et al. report a sensitivity of 33% as well using ^{68}Ga -PSMA PET/CT (31). Maurer et al. demonstrated that ^{68}Ga -PSMA PET/CT was significantly better in detecting metastatic LNs than conventional imaging (CT or MRI) in 130 patients with primary intermediate- or high-grade PCa. Thirty-one percent of patients presented with LN metastases at histology, and ^{68}Ga -PSMA PET/CT had a patient-based sensitivity of 66%, specificity of 99%, and accuracy of 88%. In an LN field-based analysis (16% of 117 LN field positive at histology) sensitivity, specificity, and accuracy of ^{68}Ga -PSMA PET/CT were 68%, 99%, and 95%, respectively (32). When patients who were being treated with ADT in our study population were excluded, sensitivity increased to 50%. ADT may therefore be seen as a negative factor for visualizing of LNI. This finding appears to contradict findings that ADT may increase PSMA expression and improve detection rates of PSMA imaging (33). However, long-standing ADT also reduces tumor mass and thus the ability for PSMA imaging ligands to visualize now much smaller lesions. Thus, we believe this explains the reduced diagnostic performance of ^{99m}Tc -trofolostat SPECT/CT in our patients who had been receiving ADT for much longer than 7 d before SPECT imaging. Furthermore, we show that ^{99m}Tc -trofolostat uptake in the prostate lesion itself is a predictor of LNI, with a good sensitivity of 90%, but a somewhat lower specificity of 67% using a TBR of 30.2.

In the current study, only a small number of patients with low GS were present. It will therefore be important to study the performance of ^{99m}Tc -trofolostat SPECT/CT in a larger cohort of patients with low-risk PCa, especially because it may be a useful tool for active surveillance in these patients, ultimately determining which patients have to be moved to active treatment when uptake in the lesion increases, representing a higher GS or progressing lesion. Likewise, only patients with primary PCa were included in this study. Recent data have shown, however, the large potential of PSMA-targeted imaging in restaging patients with biochemical recurrence after initial curative treatment (13,34), using ^{68}Ga -labeled compounds and PET imaging. PET/CT cameras are, however, not widely

available in general hospitals and the cost of a ^{68}Ga generator is high, demonstrating the remaining need for an easily produced ^{99m}Tc -labeled PSMA agent that can be imaged using SPECT. The usefulness of ^{99m}Tc -trofolostat imaging of biochemical recurrence, however, still needs to be proven but shows potential in this setting. Similarly, ^{99m}Tc -trofolostat SPECT/CT can also be used as a baseline staging tool in patients with disseminated disease who are candidates for PSMA-based radionuclide treatment such as ^{131}I -MIP 1095 (35) or ^{177}Lu -labeled compounds (36).

CONCLUSION

^{99m}Tc -trofolostat SPECT/CT imaging is able to detect primary PCa with high accuracy, as demonstrated in this multicenter phase 2 study. Its uptake within the prostate lesion is correlated to GS and may predict LN involvement in patients with intermediate- and high-risk PCa compared with histology. Further studies in other patient populations are warranted to evaluate the broader applicability of this promising PSMA-based imaging agent.

DISCLOSURE

Molecular Insight Pharmaceuticals, Inc. (a wholly owned subsidiary of Progenics Pharmaceuticals), Tarrytown, NY, USA, had a role in sponsoring the data and material in the study. Thomas Armor, Nancy Stambler, Vivien Wong, and Thomas Strack are full-time employees of Progenics Pharmaceuticals. Nancy Stambler and Vivien Wong are shareholders of Progenics Pharmaceuticals, Inc. No other potential conflict of interest relevant to this article was reported.

ACKNOWLEDGMENTS

We thank William Ellis, Boris Alekseev, Istvan Buzogány, Sergey Mishugin, Jozef Stolz, Vladimir Student, Vsevolod Matveev, R. Jeffrey Karnes, Douglas Sherr, Bertam Yuh, Thomas Keane, David Jarrard, Edouard J. Trabulsi, Alberto Briganti, Oleg Karyakin, and Mila Hora for their help in acquiring the ^{99m}Tc -trofolostat SPECT/CT imaging and performing surgery.

REFERENCES

- Murphy G, Haider M, Ghai S, Sreeharsha B. The expanding role of MRI in prostate cancer. *AJR*. 2013;201:1229–1238.
- Mapelli P, Picchio M. Initial prostate cancer diagnosis and disease staging: the role of choline-PET-CT. *Nat Rev Urol*. 2015;12:510–518.
- Kratochwil C, Giesel FL, Eder M, et al. [^{177}Lu]lutetium-labelled PSMA ligand-induced remission in a patient with metastatic prostate cancer. *Eur J Nucl Med Mol Imaging*. 2015;42:987–988.
- Smith-Jones PM, Vallabahajosula S, Goldsmith SJ, et al. In vitro characterization of radiolabeled monoclonal antibodies specific for the extracellular domain of prostate-specific membrane antigen. *Cancer Res*. 2000;60:5237–5243.
- Kinoshita Y, Kuratsukuri K, Landas S, et al. Expression of prostate-specific membrane antigen in normal and malignant human tissues. *World J Surg*. 2006;30:628–636.
- Murphy GP, Elgamil AA, Su SL, Bostwick DG, Holmes EH. Current evaluation of the tissue localization and diagnostic utility of prostate specific membrane antigen. *Cancer*. 1998;83:2259–2269.
- Ghosh A, Heston WD. Tumor target prostate specific membrane antigen (PSMA) and its regulation in prostate cancer. *J Cell Biochem*. 2004;91:528–539.
- Henry MD, Wen S, Silva MD, Chandra S, Milton M, Worland PJ. A prostate-specific membrane antigen-targeted monoclonal antibody-chemotherapeutic conjugate designed for the treatment of prostate cancer. *Cancer Res*. 2004;64:7995–8001.
- Elsässer-Beile U, Buhler P, Wolf P. Targeted therapies for prostate cancer against the prostate specific membrane antigen. *Curr Drug Targets*. 2009;10:118–125.

10. Elsässer-Beile U, Reischl G, Wiehr S, et al. PET imaging of prostate cancer xenografts with a highly specific antibody against the prostate-specific membrane antigen. *J Nucl Med.* 2009;50:606–611.
11. Milowsky MI, Nanus DM, Kostakoglu L, Vallabhajosula S, Goldsmith SJ, Bander NH. Phase I trial of yttrium-90-labeled anti-prostate-specific membrane antigen monoclonal antibody J591 for androgen-independent prostate cancer. *J Clin Oncol.* 2004;22:2522–2531.
12. Eder M, Schafer M, Bauder-Wust U, et al. ⁶⁸Ga-complex lipophilicity and the targeting property of a urea-based PSMA inhibitor for PET imaging. *Bioconjug Chem.* 2012;23:688–697.
13. Afshar-Oromieh A, Avtzi E, Giesel FL, et al. The diagnostic value of PET/CT imaging with the ⁶⁸Ga-labelled PSMA ligand HBED-CC in the diagnosis of recurrent prostate cancer. *Eur J Nucl Med Mol Imaging.* 2015;42:197–209.
14. Eiber M, Maurer T, Souvatzoglou M, et al. Evaluation of hybrid ⁶⁸Ga-PSMA ligand PET/CT in 248 patients with biochemical recurrence after radical prostatectomy. *J Nucl Med.* 2015;56:668–674.
15. Szabo Z, Mena E, Rowe SP, et al. Initial Evaluation of [¹⁸F]DCFPyL for prostate-specific membrane antigen (PSMA)-targeted PET imaging of prostate cancer. *Mol Imaging Biol.* 2015;17:565–574.
16. Hillier SM, Maresca KP, Lu G, et al. ^{99m}Tc-labeled small-molecule inhibitors of prostate-specific membrane antigen for molecular imaging of prostate cancer. *J Nucl Med.* 2013;54:1369–1376.
17. Barrett JA, Coleman RE, Goldsmith SJ, et al. First-in-man evaluation of 2 high-affinity PSMA-avid small molecules for imaging prostate cancer. *J Nucl Med.* 2013;54:380–387.
18. Robu S, Schottelius M, Eiber M, et al. Preclinical evaluation and first patient application of ^{99m}Tc-PSMA-I&S for SPECT imaging and radioguided surgery in prostate cancer. *J Nucl Med.* 2017;58:235–242.
19. Vallabhajosula S, Nikolopoulou A, Babich JW, et al. ^{99m}Tc-labeled small-molecule inhibitors of prostate-specific membrane antigen: pharmacokinetics and biodistribution studies in healthy subjects and patients with metastatic prostate cancer. *J Nucl Med.* 2014;55:1791–1798.
20. Godoy G, Chong KT, Cronin A, et al. Extent of pelvic lymph node dissection and the impact of standard template dissection on nomogram prediction of lymph node involvement. *Eur Urol.* 2011;60:195–201.
21. Eiber M, Weirich G, Holzzapfel K, et al. Simultaneous Ga-PSMA HBED-CC PET/MRI improves the localization of primary prostate cancer. *Eur Urol.* 2016;70:829–836.
22. Giesel FL, Sterzing F, Schlemmer HP, et al. Intra-individual comparison of Ga-PSMA-11-PET/CT and multi-parametric MR for imaging of primary prostate cancer. *Eur J Nucl Med Mol Imaging.* 2016;43:1400–1406.
23. Rowe SP, Gage KL, Faraj SF, et al. ¹⁸F-DCFBC PET/CT for PSMA-based detection and characterization of primary prostate cancer. *J Nucl Med.* 2015;56:1003–1010.
24. Perner S, Hofer MD, Kim R, et al. Prostate-specific membrane antigen expression as a predictor of prostate cancer progression. *Hum Pathol.* 2007;38:696–701.
25. Rahbar K, Weckesser M, Huss S, et al. Correlation of intraprostatic tumor extent with ⁶⁸Ga-PSMA distribution in patients with prostate cancer. *J Nucl Med.* 2016;57:563–567.
26. Uprimny C, Kroiss AS, Decristoforo C, et al. ⁶⁸Ga-PSMA-11 PET/CT in primary staging of prostate cancer: PSA and Gleason score predict the intensity of tracer accumulation in the primary tumour. *Eur J Nucl Med Mol Imaging.* 2017;44:941–949.
27. Zamboglou C, Wieser G, Hennes S, et al. MRI versus ⁶⁸Ga-PSMA PET/CT for gross tumour volume delineation in radiation treatment planning of primary prostate cancer. *Eur J Nucl Med Mol Imaging.* 2016;43:889–897.
28. Barentsz JO, Richenberg J, Clements R, et al. ESUR prostate MR guidelines 2012. *Eur Radiol.* 2012;22:746–757.
29. Claus FG, Hricak H, Hattery RR. Pretreatment evaluation of prostate cancer: role of MR imaging and ¹H MR spectroscopy. *Radiographics.* 2004;24(suppl 1):S167–S180.
30. Choi YJ, Kim JK, Kim N, Kim KW, Choi EK, Cho KS. Functional MR imaging of prostate cancer. *Radiographics.* 2007;27:63–75.
31. Budäus L, Leyh-Bannurah SR, Salomon G, et al. Initial experience of ⁶⁸Ga-PSMA PET/CT imaging in high-risk prostate cancer patients prior to radical prostatectomy. *Eur Urol.* 2016;69:393–396.
32. Maurer T, Gschwend JE, Rauscher I, et al. Diagnostic efficacy of ⁶⁸Ga-PSMA positron emission tomography compared to conventional imaging for lymph node staging of 130 consecutive patients with intermediate to high risk prostate cancer. *J Urol.* 2016;195:1436–1443.
33. Hope TA, Truillet CC, Ehman EC, et al. Imaging response to androgen receptor inhibition using ⁶⁸Ga-PSMA-11 PET: first human experience. *J Nucl Med.* 2017;58:81–84.
34. Eiber M, Nekolla SG, Maurer T, Weirich G, Wester HJ, Schwaiger M. ⁶⁸Ga-PSMA PET/MR with multimodality image analysis for primary prostate cancer. *Abdom Imaging.* 2015;40:1769–1771.
35. Zechmann CM, Afshar-Oromieh A, Armor T, et al. Radiation dosimetry and first therapy results with a ¹²⁴I/¹³¹I-labeled small molecule (MIP-1095) targeting PSMA for prostate cancer therapy. *Eur J Nucl Med Mol Imaging.* 2014;41:1280–1292.
36. Ahmadzadehfard H, Rahbar K, Kurpig S, et al. Early side effects and first results of radioligand therapy with ¹⁷⁷Lu-DKFZ-617 PSMA of castrate-resistant metastatic prostate cancer: a two-centre study. *EJNMMI Res.* 2015;5:114.